metals

MDPI

Article

Glass Forming Ability, Magnetic Properties and Magnetocaloric Effect of the $Tb_{65}Ni_{15}Co_{20}$ Amorphous Alloy

Weihuo Li [1,2], Ying Huang [1], Qiang Wang [3], Xu Zhou [3], Ding Ding [3] and Lei Xia [3,*]

[1] School of Materials Science and Engineering, Key Laboratory of Green Fabrication and Surface Technology of Advanced Metal Materials, Ministry of Education, Anhui University of Technology, Maanshan 243032, China
[2] Wuhu Technology and Innovation Research Institute, Anhui University of Technology, Wuhu 241000, China
[3] Institute of Materials, Shanghai University, Shanghai 200072, China
* Correspondence: xialei@shu.edu.cn; Tel.: +86-021-66135067

Abstract: In the paper, $Tb_{65}Ni_{35-x}Co_x$ (x = 0, 10, 20, 30) amorphous ribbons were successfully prepared, and the glass-forming ability (GFA) of these ribbons was investigated. Both the T_{rg} and γ of the $Tb_{65}Ni_{35-x}Co_x$ amorphous ribbons were larger than those of the $Tb_{65}Ni_{35}$ alloy and reached the maximum when x = 20, indicating that the $Tb_{65}Ni_{15}Co_{20}$ amorphous alloy has an optimal GFA. The magnetic properties as well as magnetocaloric effect of the $Tb_{65}Ni_{15}Co_{20}$ amorphous alloy were studied. The Curie temperature (T_c) of the amorphous alloy was ~79 K and the typical spin-glass-like behavior was found in the alloy. The peak value of magnetic entropy change ($-\Delta S_m{}^{peak}$) for the amorphous alloy was up to 9.47 J kg^{-1} K^{-1} under 5 T. The mechanism for the increased T_c and enlarged $-\Delta S_m{}^{peak}$ of the $Tb_{65}Ni_{15}Co_{20}$ amorphous alloy was analyzed.

Keywords: metallic glass; glass-forming ability; magnetocaloric effect; magnetic entropy change

Citation: Li, W.; Huang, Y.; Wang, Q.; Zhou, X.; Ding, D.; Xia, L. Glass Forming Ability, Magnetic Properties and Magnetocaloric Effect of the $Tb_{65}Ni_{15}Co_{20}$ Amorphous Alloy. *Metals* **2022**, *12*, 1399. https://doi.org/10.3390/met12091399

Academic Editor: Imre Bakonyi

Received: 7 August 2022
Accepted: 18 August 2022
Published: 23 August 2022

1. Introduction

With the increasing problems of energy consumption and air pollution, it is very necessary to develop new refrigeration methods to replace the traditional refrigeration technology using freon as a refrigerant. Among these refrigeration technologies, the magnetic refrigeration (MR) method, which is based on the magnetocaloric effect (MCE), has attracted more interest over the past several decades [1,2]. Compared with traditional vapor compression cycle refrigeration technology, MR possesses the advantages of high efficiency (as high as 30–60%, but the traditional refrigeration efficiency is only 5–10%), free of greenhouse gas and more compactness due to the use of solid refrigerant [1–5]. The performance of a magnetic refrigeration equipment fundamentally depends on the MCE of its refrigerant; thus, it is significant to choose appropriate refrigeration materials.

At present, the magnetic materials that exhibit MCE can be divided into two categories: (1) Crystalline compounds undergoing a first-order magnetic phase transition (FOMPT) usually show ultra-high magnetic entropy change peak ($-\Delta S_m{}^{peak}$), but this ultra-high $-\Delta S_m{}^{peak}$ only exists within a very narrow temperature range, such as Gd-Si-Ge-, La-Fe-Si- and Ni-Mn-based alloys [6–10]. (2) The MCE materials undergoing a second-order magnetic phase transition (SOMPT), represented by pure Gd metal and amorphous alloys (AAs), exhibit relatively lower $-\Delta S_m{}^{peak}$ than FOMPT materials [11–14]. However, the magnetic entropy change ($-\Delta S_m$) curves of the SOMPT MCE materials are broader, which means they can operate in a wide temperature range and, thus, leads to a much larger refrigeration capacity. Therein, AAs can be formed within a wide compositional range and can easily tune their Curie temperature (T_c) and $-\Delta S_m{}^{peak}$ by compositional adjustment [15–17]. In addition, compared with the crystalline alloys, AAs also have better mechanical properties, higher corrosion resistance and lower eddy current losses [18,19]. Therefore, amorphous MCE alloys may be more suitable candidates as magnetic refrigerants used in magnetic refrigeration.

Among amorphous MCE alloys, rare earth (RE)-transition metal (TM)-based AAs and TM-based AAs are the main two categories. The TM-based amorphous MCE alloys usually show very low $-\Delta S_m^{peak}$ (not exceed 4.0 J kg^{-1} K^{-1} under 5 T) [3,20–22]. Instead, the magnetocaloric effect of the RE-TM-based AAs are quite excellent, especially in Gd-TM-based AAs [23–29]. For example, a $-\Delta S_m^{peak}$ under 5 T of up to 11.06 J kg^{-1} K^{-1} was achieved in a ternary $Gd_{34}Ni_{33}Al_{33}$ metallic glass [24]; $Gd_{55\text{-}60}Co_{15\text{-}30}Al_{15\text{-}30}$ AAs exhibited the $-\Delta S_m^{peak}$ of 8.6~9.6 J kg^{-1} K^{-1} under 5 T [25]. In recent reports, other RE-TM-based (such as Nd, Tb and Dy) AAs also showed rather high $-\Delta S_m^{peak}$. The $-\Delta S_m^{peak}$ under 5 T of $Nd_{65}Co_{35}$ AA reached 7.59 J kg^{-1} K^{-1} [26]. The Tb/Dy-TM AAs even showed a $-\Delta S_m^{peak}$ comparable to those of Gd-based metallic glasses [27–29]. Thus, it is important for the application of MR to develop and improve the $-\Delta S_m^{peak}$ of the RE-TM-based AAs as high as possible.

In previous work, we have systematically investigated the glass-forming ability (GFA) and magnetocaloric properties of the Tb-Ni binary alloys, and a $-\Delta S_m^{peak}$ under 5 T of 8.7 J kg^{-1} K^{-1} was obtained in the $Tb_{65}Ni_{35}$ alloy, which was the only fully amorphous sample in the binary alloys [30]. Frustratingly, the GFA of the $Tb_{65}Ni_{35}$ AA was very poor. Therefore, in order to increase the GFA and concurrently further improve the MCE of the $Tb_{65}Ni_{35}$ AA, the replacement of Ni atom with other TM atoms should be a valid way. In the present work, Co was used in the substitution of Ni to prepare $Tb_{65}Ni_{35-x}Co_x$ (x = 0, 10, 20 and 30) amorphous ribbons, and the GFA of the ternary alloys was investigated. The best glass former in the ternary alloys was employed to study its magnetic properties and MCE in detail.

2. Materials and Methods

The $Tb_{65}Ni_{35-x}Co_x$ (x = 0, 10, 20, 30) alloy ingots were produced by arc-melting the mixture of Tb, Ni and Co metals (purity > 99.9 at.%) in a high vacuum furnace under the protection of high-purity Ar atmosphere. Each master ingot was remelted in a quartz tube filled with Ar atmosphere and then the melt was injected on a copper wheel with a speed of 30 m/s to fabricate the $Tb_{65}Ni_{35-x}Co_x$ ribbons. These ribbons with a width of ~3 mm and a uniform thickness of ~40 μm were selected for the structure and performance measurements. A Rigaku D/max-2550 X-ray diffractometer (XRD, Rigaku, Tokyo, Japan) with Cu K_α radiation was employed to detect the structural information of the $Tb_{65}Ni_{35-x}Co_x$ as-spun ribbons. The thermal properties of the glassy sample were achieved from their differential scanning calorimetric (DSC) curves measured on a model 404 C calorimeter produced by NETZSCH Company (Selb, Germany). The GFA of these amorphous ribbons was evaluated according to their thermal parameters and the best glass former was determined to investigate its magnetic properties and MCE. The magnetic measurements of the amorphous ribbon with the best GFA, including magnetization vs. temperature (*M*-*T*) curves, hysteresis loops and isothermal magnetization (*M*-*H*) curves, were performed on a model 6000 Physical Property Measurement System (PPMS) produced by Quantum Design Company (San Diego, CA, USA).

3. Results and Discussion

The X-ray diffraction results of the $Tb_{65}Ni_{35-x}Co_x$ (x = 0, 10, 20, 30) as-spun ribbons are displayed in Figure 1. There were no obviously sharp crystalline peaks and only smoothly broad diffraction diffusion in their XRD patterns, which indicates the typical amorphous characteristic of these ribbons.

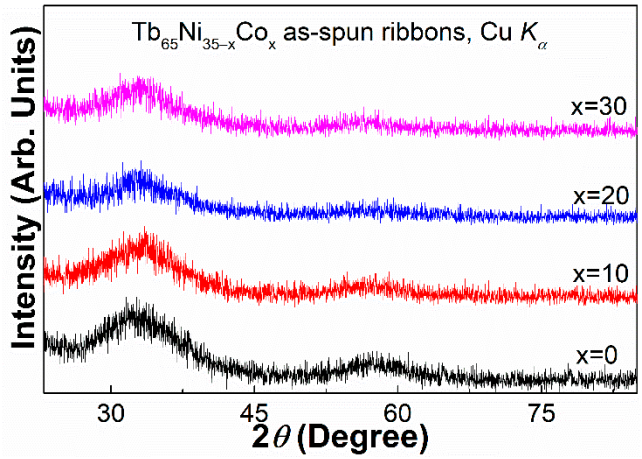

Figure 1. XRD patterns of the $Tb_{65}Ni_{35-x}Co_x$ (x = 0, 10, 20, 30) as-spun ribbons.

Figure 2a shows the DSC curves of $Tb_{65}Ni_{35-x}Co_x$ (x = 0, 10, 20, 30) amorphous ribbons. It can be seen that as the temperature rose, a faint upward endothermic peak first appeared, which corresponded to the glass transition behavior of the ribbon, following by downward exothermic crystallization peaks on each curve. This further proves the typical amorphous features of these samples. From their DSC curves and melting curves, we can obtain the temperatures of glass transition (T_g), primary crystallization temperatures (T_x) and liquidus temperatures (T_l) to evaluate the glass-forming ability of the $Tb_{65}Ni_{35-x}Co_x$ (x = 0, 10, 20, 30) AAs, as listed in Table 1. Two criteria used commonly (i.e., the reduced glass transition temperature ($T_{rg} = T_g/T_l$) [31] and parameter γ (= $T_x/(T_g + T_l)$) [32]) can be calculated accordingly. As shown in Figure 2b, both the T_{rg} and γ were larger than those of the $Tb_{65}Ni_{35}$ amorphous alloy [30], indicating that the replacement of Ni atom with Co atom can dramatically improve the GFA of the $Tb_{65}Ni_{35}$ binary alloy. In addition, the value of the T_{rg} and γ first increased and then decreased with the increase in Co content and reached the maximum value when x = 20, which implies the best glass former in the $Tb_{65}Ni_{35-x}Co_x$ ternary alloys was $Tb_{65}Ni_{15}Co_{20}$.

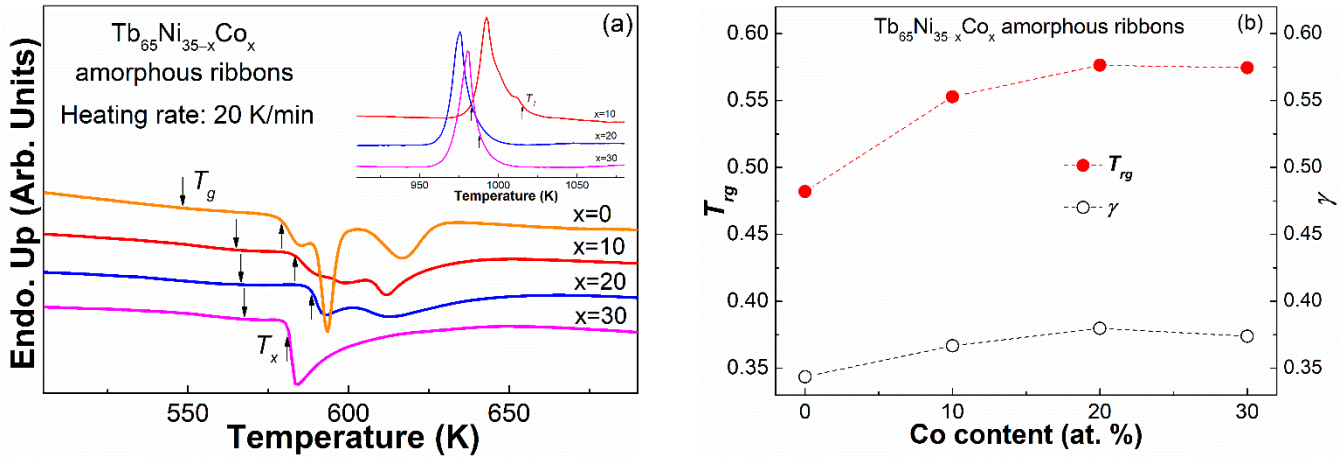

Figure 2. (**a**) DSC curves of the $Tb_{65}Ni_{35-x}Co_x$ (x = 0, 10, 20 and 30) amorphous ribbons at a heating rate of 0.333 K/s, and the inset are the melting behaviors; (**b**) the compositional dependence of T_{rg} and γ for the $Tb_{65}Ni_{35-x}Co_x$ amorphous ribbons.

Table 1. Thermal parameters, T_{rg} and γ of the $Tb_{65}Ni_{35-x}Co_x$ (x = 0, 10, 20 and 30) amorphous alloys.

$Tb_{65}Ni_{35-x}Co_x$	T_g (K)	T_x (K)	T_l (K)	T_{rg}	γ
x = 0	548	579	1137	0.482	0.344
x = 10	565	582	1022	0.553	0.367
x = 20	566	588	982	0.576	0.380
x = 30	567	581	987	0.574	0.374

Figure 3a shows the variation of magnetization with temperature under 0.03 T for the $Tb_{65}Ni_{15}Co_{20}$ glassy ribbon after two different cooling treatments from room temperature to 10 K, i.e., zero-field-cooling (ZFC) and field-cooling (FC). Obviously, as the temperature decreased, the ZFC and FC *M*-*T* curves were almost coincident at first, and until a certain temperature (~64 K), the two curves begin to deviate. The λ-shaped *M*-*T* curves usually occur in the spin-glass systems and other spin-glass-like metallic glass [26,28–30,33], indicating the typical spin-glass-like behavior of the $Tb_{65}Ni_{15}Co_{20}$ glassy alloy. The T_c and spin freezing temperature (T_f) were obtained to be ~79 K and ~64 K by derivating the *M*-*T* curves of the glassy sample. The increased T_c of the $Tb_{65}Ni_{15}Co_{20}$ glassy ribbon than the $Tb_{65}Ni_{35}$ amorphous ribbon (T_c = 64 K) may be closely related to the enhanced 3*d*-3*d* interaction between TM atoms because the magnetic moment of Co is larger than that of Ni. Similar to some RE (such as Nd, Tb and Dy)-based metallic glasses [26–28,30], the spin-glass-like behavior resulted in large coercivity (H_c) and magnetic hysteresis at low temperatures below T_f. Hence, the hysteresis loops of the $Tb_{65}Ni_{15}Co_{20}$ AA at 10, 70 and 160 K were measured as illustrated in Figure 3b. The amorphous sample shows hard magnetic with a H_c of 0.624 T at 10 K (well lower than T_f), soft magnetic at 70 K (between T_f and T_c) and paramagnetic at 160 K (well above T_c).

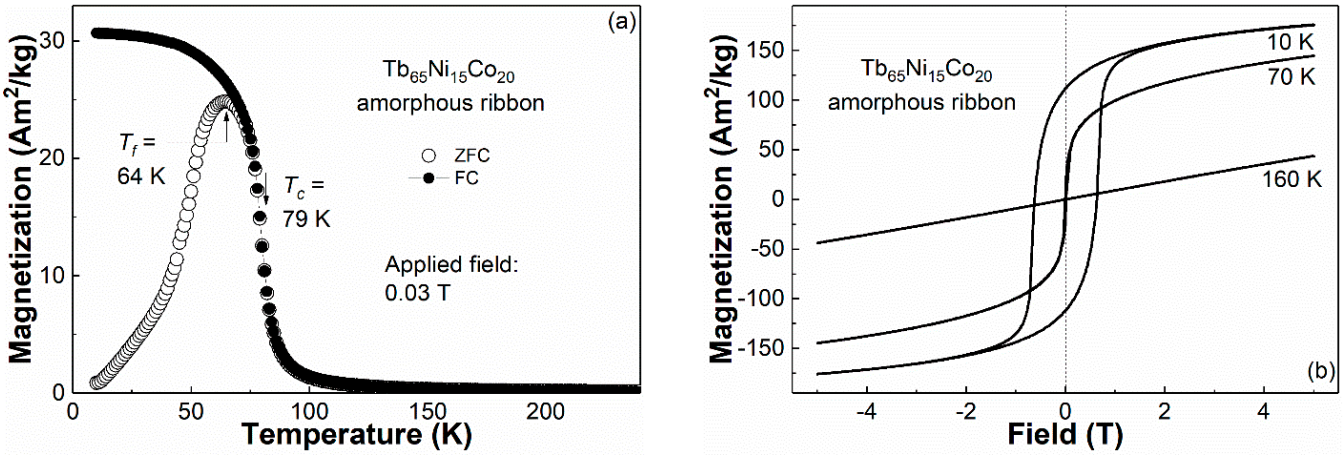

Figure 3. (**a**) FC and ZFC *M*-*T* curves of the $Tb_{65}Ni_{15}Co_{20}$ amorphous ribbon under a magnetic field of 0.03 T; (**b**) the hysteresis loops of the amorphous ribbon measured at 10, 70 and 160 K. (The magnetization can be transformed to be SI unit according to 1 $Am^2/kg \approx 120$ A/m).

The large coercivity even inhibited the magnetization of the alloy at low temperature and, thus, brought about the abnormal magnetization phenomena. Figure 4 shows the *M*-*H* curves of the $Tb_{65}Ni_{15}Co_{20}$ glassy alloy at various temperatures from 0 to 5 T. At temperatures above T_f, the magnetization of the ribbon increased with the decrease in the temperature. However, the magnetization showed a positive correlation with the temperature under an extreme low magnetic field, when the temperature was below T_f, especially at 10 K, which also implies the spin-glass-like behavior of the $Tb_{65}Ni_{15}Co_{20}$ glassy sample.

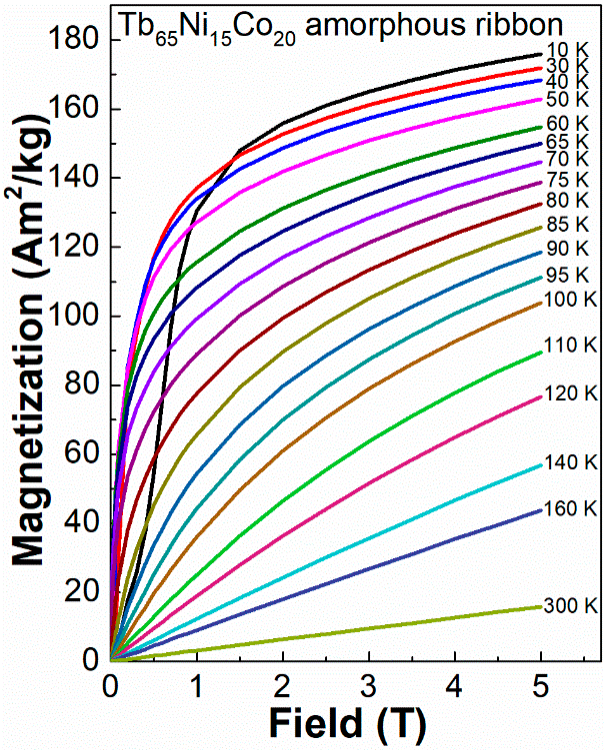

Figure 4. The isothermal *M*-*H* curves of the $Tb_{65}Ni_{15}Co_{20}$ amorphous ribbon measured at various temperatures under a magnetic field of 5 T.

It is known that the abnormal magnetization behavior induced by the inhibition of the coercivity will affect the magnetocaloric properties of the AAs [26,30,34,35]. As such, we obtained the $-\Delta S_m$ of the $Tb_{65}Ni_{15}Co_{20}$ amorphous ribbon under different magnetic fields and temperatures according to Maxwell's equation. Figure 5a displays the relationship between $-\Delta S_m$ and temperature ($-\Delta S_m$-T curves) under 1 T, 1.5 T, 2 T, 3 T, 4 T and 5 T for the $Tb_{65}Ni_{15}Co_{20}$ glassy ribbon. Similar with the situation in the spin-glass-like AAs, the $-\Delta S_m$ of the sample even decreases to a negative value at the temperatures below 30 K, which implies the irreversible magnetocaloric effect of the $Tb_{65}Ni_{15}Co_{20}$ glassy alloy. As the temperature rose, the $-\Delta S_m$ first increased and then decreased to near zero and reached a maximum $-\Delta S_m$ at the vicinity of T_c. The value of $-\Delta S_m{}^{peak}$ for the $Tb_{65}Ni_{15}Co_{20}$ amorphous ribbon was 2.70 J kg^{-1} K^{-1} under 1 T, 3.79 J kg^{-1} K^{-1} under 1.5 T, 4.75 J kg^{-1} K^{-1} under 2 T, 6.48 J kg^{-1} K^{-1} under 3 T, 8.05 J kg^{-1} K^{-1} under 4 T and 9.47 J kg^{-1} K^{-1} under 5 T. On the other hand, according to the $-\Delta S_m{}^{peak}$ under different magnetic fields (H), the $\ln(-\Delta S_m{}^{peak})$ vs. $\ln(H)$ plots of the $Tb_{65}Ni_{15}Co_{20}$ amorphous ribbon can be constructed, which is proposed by V. Franco [36]. The slope (defined as n) of its linear fitting curve near T_c, as displayed in the inset of Figure 5a, was 0.776 and agreed well with the experimental value in some AAs experiencing SOMPT.

Compared with the binary $Tb_{65}Ni_{35}$ AA [30], the MCE of the TbNi(Co) glassy alloy was improved obviously by replacing Ni atoms with Co atoms. Figure 5b illustrates the $-\Delta S_m$-T curves under 1.5 T and 5 T for the $Tb_{65}Ni_{35}$ and $Tb_{65}Ni_{15}Co_{20}$ amorphous ribbons. The addition of 20 at.% Co atoms not only increased the $-\Delta S_m{}^{peak}$ temperature of the $Tb_{65}Ni_{35}$ AA, but also made the $-\Delta S_m{}^{peak}$ under 1.5 T and 5 T of the $Tb_{65}Ni_{35}$ glassy alloy enlarge by 15.9% and 8.2%, respectively. The enlarged $-\Delta S_m{}^{peak}$ induced by the substitution of Ni atoms with Co atoms was likely due to the additional 3*d*-3*d* interaction between Ni and Co atoms [37].

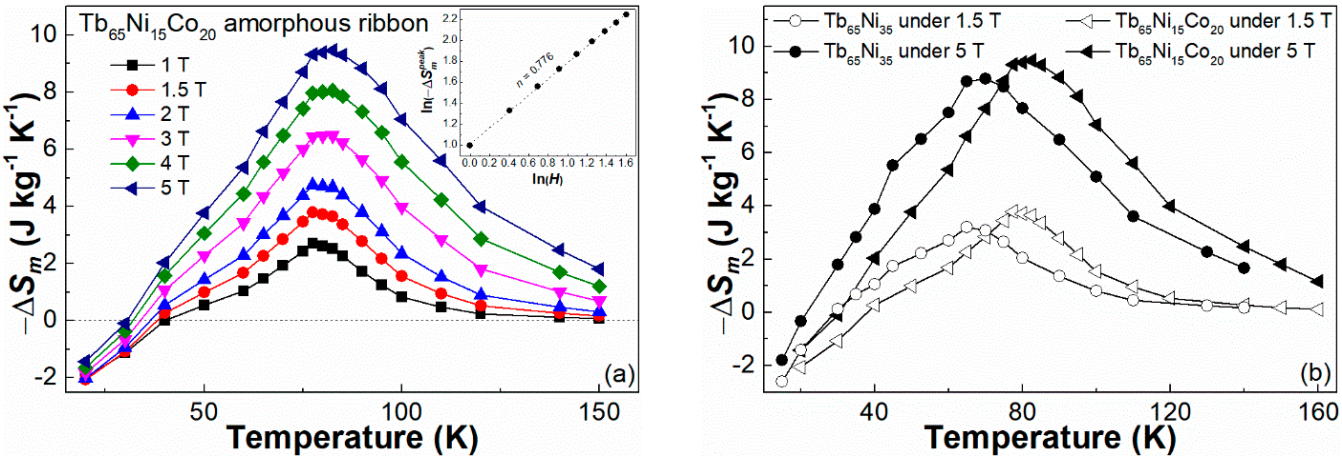

Figure 5. (**a**) The $-\Delta S_m$-T curves of the $Tb_{65}Ni_{15}Co_{20}$ amorphous ribbon under different magnetic fields, the inset is the linear fitting of the $\ln(-\Delta S_m{}^{peak})$ vs. $\ln(H)$ plots; (**b**) the $-\Delta S_m$-T curves of the $Tb_{65}Ni_{35}$ and $Tb_{65}Ni_{15}Co_{20}$ amorphous ribbons under 1.5 T and 5 T.

The adiabatic temperature change as a function of temperature (ΔT_{ad}-T curves) for the $Tb_{65}Ni_{15}Co_{20}$ amorphous ribbon under various magnetic fields were estimated from its $-\Delta S_m$-T and $C_p(T)$ curve according to:

$$\Delta T_{ad}(T,\ 0 \rightarrow H) = -\frac{T}{C_p(T)}\Delta S_m(T,\ 0 \rightarrow H)$$

Figure 6 illustrates the ΔT_{ad}-T curves under 1 T to 5 T of the $Tb_{65}Ni_{15}Co_{20}$ amorphous ribbon, and the inset shows its $C_p(T)$ curve. The maximum ΔT_{ad} of the sample is approximately 1.14 K under 1 T, 2.12 K under 2 T, 2.94 K under 3 T, 3.73 K under 4 T, and 4.47 K under 5 T, all of which are comparable to some crystal magnetic refrigeration materials with a giant MCE [10,38]. Furthermore, the large $-\Delta S_m{}^{peak}$ and ΔT_{ad} (9.47 J kg^{-1} K^{-1} and 4.47 K under 5 T) of the $Tb_{65}Ni_{15}Co_{20}$ amorphous ribbon are higher than those of most Gd-based MCE AAs [12,24,25,39–41], and amorphous alloys possess better mechanical properties and corrosion resistance than intermetallic compounds [42], both of which jointly indicate the application perspective of the amorphous alloy as the magnetic refrigerants in magnetic refrigeration near the liquefaction temperature of nitrogen.

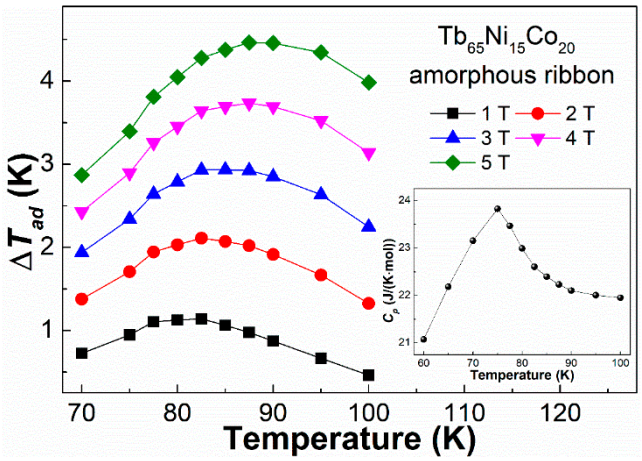

Figure 6. The ΔT_{ad}-T curves of the $Tb_{65}Ni_{15}Co_{20}$ amorphous ribbon under different magnetic fields, the inset is the $C_p(T)$ plots.

4. Conclusions

In summary, we prepared the $Tb_{65}Ni_{35-x}Co_x$ (x = 0, 10, 20, 30) amorphous ribbons by replacing Ni atoms with Co atoms, and the GFA of the ternary alloys was studied. The results show that the addition of Co atoms obviously improves the GFA of the $Tb_{65}Ni_{35}$ AA, and the T_{rg} as well as γ reach to the maximum value when x = 20, which indicates the best glass former is $Tb_{65}Ni_{15}Co_{20}$. The magnetic properties and MCE of the $Tb_{65}Ni_{15}Co_{20}$ glassy ribbon were further investigated. The λ-shaped *M-T* curves as well as the anomalous *M-H* curves at low field and low temperature indicate the spin-glass-like behavior of the $Tb_{65}Ni_{15}Co_{20}$ AA, with a T_f of ~64 K and a T_c of ~79 K. The large coercivity (~0.624 T at 10 K) of the AA results in the irreversible $-\Delta S_m$ at the temperatures well below T_f. The $-\Delta S_m{}^{peak}$ and ΔT_{ad} under 5 T of the $Tb_{65}Ni_{15}Co_{20}$ amorphous ribbon reach to 9.47 J K^{-1} kg^{-1} and 4.47 K, both of which were larger than that of most Gd-based AAs, indicating a promising perspective in the application of magnetic refrigeration. Compared with the $Tb_{65}Ni_{35}$ glassy alloy, the increased T_c and enlarged $-\Delta S_m{}^{peak}$ of the $Tb_{65}Ni_{15}Co_{20}$ amorphous ribbon may be closely related to the extra 3*d*-3*d* interaction between Ni and Co atoms due to the addition of Co atoms with larger magnetic moment.

Author Contributions: Conceptualization, W.L. and L.X.; methodology, D.D.; investigation, Y.H., Q.W. and X.Z.; data curation, Q.W. and X.Z.; writing—original draft preparation, W.L., Q.W. and X.Z.; writing—review and editing, L.X.; funding acquisition, L.X. All authors have read and agreed to the published version of the manuscript.

Funding: This research was funded by the National Natural Science Foundation of China (grant numbers: 51871139 and 52071196) and Key Research & Development plan of Anhui Province (grant numbers: 2022a05020016).

Institutional Review Board Statement: Not applicable.

Informed Consent Statement: Not applicable.

Data Availability Statement: Not applicable.

Acknowledgments: This research was technically supported by the Center for Advanced Microanalysis of Shanghai University.

Conflicts of Interest: The authors declare no conflict of interest.

References

1. de Oliveira, N.A.; von Ranke, P.J. Theoretical aspects of the magnetocaloric effect. *Phys. Rep.* **2010**, *489*, 89–159. [CrossRef]
2. Tishin, A.M.; Spichkin, Y.I. *The Magnetocaloric Effect and Its Applications*; IOP: Bristol, UK, 2003.
3. Franco, V.; Blázquez, J.S.; Ipus, J.J.; Law, J.Y.; Moreno-Ramírez, L.M.; Conde, A. Magnetocaloric effect: From materials research to refrigeration devices. *Prog. Mater. Sci.* **2018**, *93*, 112–232. [CrossRef]
4. Pecharsky, V.K.; Gschneidner, K.A., Jr. Magnetocaloric effect and magnetic refrigeration. *J. Magn. Magn. Mater.* **1999**, *200*, 44–56. [CrossRef]
5. Brück, E. Developments in magnetocaloric refrigeration. *J. Phys. D Appl. Phys.* **2005**, *38*, R381–R391. [CrossRef]
6. Pecharsky, V.K.; Gschneidner, K.A., Jr. Giant Magnetocaloric Effect in $Gd_5(Si_2Ge_2)$. *Phys. Rev. Lett.* **1997**, *78*, 4494–4497. [CrossRef]
7. Hu, F.X.; Shen, B.G.; Sun, J.R.; Cheng, Z.H.; Rao, G.H.; Zhang, X.X. Influence of negative lattice expansion and metamagnetic transition on magnetic entropy change in the compound $LaFe_{11.4}Si_{1.6}$. *Appl. Phys. Lett.* **2001**, *78*, 3675–3677. [CrossRef]
8. Han, Z.D.; Wang, D.H.; Zhang, C.L.; Tang, S.L.; Gu, B.X.; Du, Y.W. Large magnetic entropy changes in the $Ni_{45.4}Mn_{41.5}In_{13.1}$ ferromagnetic shape memory alloy. *Appl. Phys. Lett.* **2006**, *89*, 182507. [CrossRef]
9. Chaudhary, V.; Chen, X.; Ramanujan, R.V. Iron and manganese based magnetocaloric materials for near room temperature thermal management. *Prog. Mater. Sci.* **2019**, *100*, 64–98. [CrossRef]
10. Zarkevich, N.A.; Zverev, V.I. Viable Materials with a Giant Magnetocaloric Effect. *Crystals* **2020**, *10*, 815. [CrossRef]
11. Dankov, S.Y.; Tishin, A.M.; Pecharsky, V.K.; Gschneidner, K.A. Magnetic phase transitions and the magnetothermal properties of gadolinium. *Phys. Rev. B* **1998**, *57*, 3478. [CrossRef]
12. Luo, Q.; Zhao, D.Q.; Pan, M.X.; Wang, W.H. Magnetocaloric effect in Gd-based bulk metallic glasses. *Appl. Phys. Lett.* **2006**, *89*, 081914. [CrossRef]
13. Luo, Q.; Wang, W.H. Rare earth based bulk metallic glasses. *J. Non-Cryst. Solids* **2009**, *355*, 759–775. [CrossRef]
14. Zverev, V.I.; Tishin, A.M.; Kuz'min, M.D. The maximum possible magnetocaloric ΔT effect. *J. Appl. Phys.* **2010**, *107*, 043907. [CrossRef]

15. Wu, C.; Ding, D.; Xia, L.; Chan, K.C. Achieving tailorable magneto-caloric effect in the Gd-Co binary amorphous alloys. *AIP Adv.* **2016**, *6*, 035302. [CrossRef]
16. Yin, H.B.; Law, J.Y.; Huang, Y.Y.; Franco, V.; Shen, H.X.; Jiang, S.D.; Bao, Y.; Sun, J.F. Design of Fe-containing GdTbCoAl high-entropy-metallic-glass composite microwires with tunable Curie temperatures and enhanced cooling efficiency. *Mater. Design* **2021**, *206*, 109824. [CrossRef]
17. Zhang, Z.Y.; Tang, Q.; Wang, F.C.; Zhang, H.Y.; Zhou, Y.X.; Xia, A.L.; Li, H.L.; Chen, S.S.; Li, W.H. Tailorable magnetocaloric effect by Fe substitution in Gd-(Co, Fe) amorphous alloy. *Intermetallics* **2019**, *111*, 106500. [CrossRef]
18. Inoue, A.; Takeuchi, A. Recent development and application products of bulk glassy alloys. *Acta Mater.* **2011**, *59*, 2243–2267. [CrossRef]
19. Li, H.X.; Lu, Z.C.; Wang, S.L.; Wu, Y.; Lu, Z.P. Fe-based bulk metallic glasses: Glass formation, fabrication, properties and applications. *Prog. Mater. Sci.* **2019**, *103*, 235–318. [CrossRef]
20. Chen, L.S.; Zhang, J.Z.; Wen, L.; Yu, P.; Xia, L. Outstanding magnetocaloric effect of $Fe_{88-x}Zr_8B_4Sm_x$ (x=0, 1, 2, 3) amorphous alloys. *Sci. China-Phys. Mech. Astron.* **2018**, *61*, 056121. [CrossRef]
21. Wang, Q.; Pan, L.L.; Tang, B.Z.; Ding, D.; Xia, L. Outstanding magnetocaloric properties at ambient temperature of a $Fe_{88}La_4Ce_3B_5$ amorphous alloy. *J. Non-Cryst. Solids* **2022**, *580*, 121394. [CrossRef]
22. Zhou, X.; Wang, Q.; Pan, L.L.; Ding, D.; Tang, B.Z.; Yu, P.; Yao, J.L.; Xia, L. Effect of Minor Co Substitution for Fe on the Formability and Magnetic and Magnetocaloric Properties of the Amorphous $Fe_{88}Ce_7B_5$ Alloy. *Metals* **2022**, *12*, 589. [CrossRef]
23. Feng, J.Q.; Liu, Y.H.; Sui, J.H.; He, A.N.; Xia, W.X.; Wang, W.H.; Wang, J.Q.; Huo, J.T. Giant refrigerant capacity in Gd-based amorphous/nanocrsytalline composite fibers. *Mater. Today Phys.* **2021**, *21*, 100528. [CrossRef]
24. Wang, X.; Wang, Q.; Tang, B.Z.; Yu, P.; Xia, L.; Ding, D. Large magnetic entropy change and adiabatic temperature rise of a ternary $Gd_{34}Ni_{33}Al_{33}$ metallic glass. *J. Rare Earth.* **2021**, *39*, 998–1002. [CrossRef]
25. Fu, H.; Zou, M. Magnetic and magnetocaloric properties of ternary Gd–Co–Al bulk metallic glasses. *J. Alloys Compd.* **2011**, *509*, 4613–4616. [CrossRef]
26. Wang, Q.; Ding, D.; Xia, L. Formability and magnetic properties of the binary Nd-Co amorphous alloys. *Metals* **2021**, *11*, 1730. [CrossRef]
27. Wang, X.; Ding, D.; Li, C.; Xia, L. Compositional dependence of curie temperature and magnetic entropy change in the amorphous Tb-Co ribbons. *Materials* **2021**, *14*, 1002. [CrossRef]
28. Ma, L.Y.; Tang, B.Z.; Chan, K.C.; Zhao, L.; Tang, M.B.; Ding, D.; Xia, L. Formability and magnetic properties of Dy-Co binary amorphous alloys. *AIP Adv.* **2018**, *8*, 075215. [CrossRef]
29. Tang, B.Z.; Guo, D.Q.; Xia, L.; Ding, D.; Chan, K.C. Magnetoelastic and magnetocaloric properties of $Tb_{62.5}Co_{37.5}$ amorphous alloy. *J. Alloys Compd.* **2017**, *728*, 747–751. [CrossRef]
30. Pan, L.L.; Wang, Q.; Zhou, X.; Tang, B.Z.; Yu, P.; Ding, D.; Xia, L. Glass formability of the Tb-Ni binary alloys and the magnetic properties of the $Tb_{65}Ni_{35}$ metallic glass. *Intermetallics* **2022**, *148*, 107650. [CrossRef]
31. Turnbull, D. Under what conditions can a glass be formed? *Contemp. Phys.* **1969**, *10*, 473–488. [CrossRef]
32. Lu, Z.; Liu, C. A new glass-forming ability criterion for bulk metallic glasses. *Acta Mater.* **2002**, *50*, 3501–3512. [CrossRef]
33. Binder, K.; Young, A.P. Spin glasses: Experimental facts, theoretical concepts, and open questions. *Rev. Mod. Phys.* **1986**, *58*, 801–976. [CrossRef]
34. Luo, Q.; Schwarz, B.; Mattern, N.; Eckert, J. Irreversible and reversible magnetic entropy change in a Dy-based bulk metallic glass. *Intermetallics* **2012**, *30*, 76–79. [CrossRef]
35. Luo, Q.; Schwarz, B.; Mattern, N.; Eckert, J. Giant irreversible positive to large reversible negative magnetic entropy change evolution in Tb-based bulk metallic glass. *Phys. Rev. B* **2010**, *82*, 024204. [CrossRef]
36. Franco, V.; Blázquez, J.S.; Conde, A. Field dependence of the magnetocaloric effect in materials with a second order phase transition: A master curve for the magnetic entropy change. *Appl. Phys. Lett.* **2006**, *89*, 222512. [CrossRef]
37. Song, M.N.; Huang, L.W.; Tang, B.Z.; Ding, D.; Wang, X.; Xia, L. Enhanced Curie temperature and magnetic entropy change of $Gd_{63}Ni_{37}$ amorphous alloy by Co substitution. *Intermetallics* **2019**, *115*, 106614. [CrossRef]
38. Singh, N.K.; Suresh, K.G.; Nigam, A.K.; Malik, S.K.; Coelho, A.A.; Gama, S. Itinerant electron metamagnetism and magnetocaloric effect in RCo_2-based Laves phase compounds. *J. Magn. Magn. Mater.* **2007**, *317*, 68–79. [CrossRef]
39. Zheng, Z.G.; Zhong, X.C.; Su, K.P.; Yu, H.Y.; Liu, Z.W.; Zeng, D.C. Magnetic properties and large magnetocaloric effects in amorphous Gd-Al-Fe alloys for magnetic refrigeration. *Sci. China-Phys. Mech. Astron.* **2011**, *54*, 1267–1270. [CrossRef]
40. Du, J.; Zheng, Q.; Li, Y.B.; Zhang, Q.; Li, D.; Zhang, Z.D. Large magnetocaloric effect and enhanced magnetic refrigeration in ternary Gd-based bulk metallic glasses. *J. Appl. Phys.* **2008**, *103*, 023918. [CrossRef]
41. Yuan, F.; Du, J.; Shen, B.L. Controllable spin-glass behavior and large magnetocaloric effect in Gd-Ni-Al bulk metallic glasses. *Appl. Phys. Lett.* **2012**, *101*, 032405. [CrossRef]
42. Zhang, H.; Gimaev, R.; Kovalev, B.; Kamilov, K.; Zverev, V.; Tishin, A. Review on the materials and devices for magnetic refrigeration in the temperature range of nitrogen and hydrogen liquefaction. *Physica B* **2019**, *558*, 65–73. [CrossRef]